PHYSICALLY DERIVED SYNTHESIS MODEL OF A CAVITY TONE

Rod Selfridge
Media and Arts Technology Doctoral College,
School of EECS
Queen Mary University of London
E1 4NS, U.K
r.selfridge@qmul.ac.uk

Joshua D Reiss
Centre for Digital Music
School of EECS
Queen Mary University of London
E1 4NS, U.K
joshua.reiss@qmul.ac.uk

Eldad J Avital
Centre for Simulation and Applied Mechanics
School of EMS
Queen Mary University of London
E1 4NS, U.K
e.avital@qmul.ac.uk

ABSTRACT

The cavity tone is the sound generated when air flows over the open surface of a cavity and a number of physical conditions are met. Equations obtained from fluid dynamics and aerodynamics research are utilised to produce authentic cavity tones without the need to solve complex computations. Synthesis is performed with a physical model where the geometry of the cavity is used in the sound synthesis calculations. The model operates in real-time making it ideal for integration within a game or virtual reality environment. Evaluation is carried out by comparing the output of our model to previously published experimental, theoretical and computational results. Results show an accurate implementation of theoretical acoustic intensity and sound propagation equations as well as very good frequency predictions.

NOMENCLATURE

c = speed of sound (m/s)
f = frequency (Hz)
ω = angular frequency = $2\pi f$ (rads/revolution)
u = air flow speed (m/s)
R_e = Reynolds number (dimensionless)
S_t = Strouhal number (dimensionless)
r = distance between listener and sound source (m)
ϕ = elevation angle between listener and sound source
φ = azimuth angle between listener and sound source
ρ_{air} = mass density of air (kgm^{-3})
μ_{air} = dynamic viscosity of air (Pa s)
M = Mach number, $M = u/c$ (dimensionless)
L = length of cavity (m)
d = depth of cavity (m)
b = width of cavity (m)
κ = wave number, $\kappa = \omega/c$ (dimensionless)
r = distance between source and listener (m)
δ = shear layer thickness (m)
δ^* = effective shear layer thickness (m)
δ_0 = shear layer thickness at edge separation (m)
θ_0 = shear layer momentum thickness at edge separation (m)
C_2 = pressure coefficient (dimensionless)

1. INTRODUCTION

Aeroacoustic sounds comprise the class of sounds generated by the movement of air past objects or edges. Alternatively, the sounds can also be generated by objects moving through the air. Examples of aeroacoustic sounds are those created when a sword swings through the air, wind passes a doorway or a spinning propellor.

Research is undertaken to accurately determine the frequencies, gain and propagation patterns required to replicate the cavity tone. Key semi-empirical formula are found within the aeroacoustic research field, allowing us to identify primary relationships and parameters. *Semi-empirical* equations are ones where an assumption or generalisation has been made to simplify the calculation or yield results in accordance with observations. Physical models have the major advantage of allowing users to continually change parameters and be confident that the underlying laws and principles are consistently obeyed, giving sounds produced an inherent authenticity.

The development of real-time sound synthesis models has great potential for use in nonlinear media such as virtual reality and games. A sound synthesis model that reacts in real-time to the variety of perspectives and interactions within these environments can offer an increased sense of realism that replaying sampled sounds may fail to capture. Linear media such as film and television may also benefit from the bespoke sound effects offered by our model. Our approach can be classified as *Procedural Audio*; sound is generated via a process dependent on evolving situations, i.e. speed of air/object motion, observer or camera position, etc. Parameters can be manipulated by a user or fully automated by a game engine producing instant changes in real-time.

The paper is organised as follows: in Section 2, we describe the state of the art for synthesising cavity sounds. The problem formulation is given in Section 3. Section 4 provides an overview of the fluid dynamics theory and equations used to predict the cavity tone. The implementation is given in detail in Section 5 with results presented in Section 6. Section 7 provides a discussion on these results including areas for future development. Finally, Section 8 concludes with a summary of our findings.

2. STATE OF THE ART

The cavity tone was synthesised in [1] in which Computational Fluid Dynamics (CFD) techniques were used to create several sound textures. The sound textures were used for real-time rendering of the audio, corresponding to air velocity and an object's motion specified by the user. The textures generated through CFD calculations can be more mathematically accurate than the equations used in this research but were not calculated in real-time due to computational complexity. Offline calculations had to be completed for each new cavity shape. This is not the case in our model.

The noise generated by jet aeroplanes was synthesised in [2]. This identifies tonal sounds generated by cavities left in the wheel wells as the landing gear is extended. An analysis approach was used to identify tonal components in aircraft noise then synthesised by using a sine wave with time varying amplitude and frequency. Perceptual tests revealed that tonal noise above 4000Hz

was extremely annoying; prediction of this along with simultaneous broadband aircraft noise is useful for aircraft engineers and designers.

Real-time sound effect synthesis using physically inspired models were presented in [3]. This includes a study into replicating the sounds generated from microscopic cavities in building walls and doorways by noise filtering. These were expressed in a "howls" model that generates filtered noise tones, triggered when the windspeed passes above a threshold. These were generalised for numerous cavities with no exact dimensions.

Often physical models of musical instruments include synthesising the coupling of vibrating air to cavities present in the instruments. Typical examples of these are [4] where a timpani model was created, and [5], which modelled stringed instruments including a Chinese Ruan. Both synthesis techniques used a finite difference methods to solve differential equations of the vibrating space; [4] using general purpose graphical processing units and [5] field programmable gate arrays to perform the computationally intensive calculations required. Our model includes the fundamental natural resonant mode of the cavity as well as tones created by a feedback mechanism. Our implementation uses equations derived from the Navier-Stokes equations but requiring much less computational power, (see Section 4.1).

Real-time synthesis of another fundamental aeroacoustic sound, the Aeolian tone was presented by the authors in [6]. The Aeolian tone is the sound generated as air flows around a solid object creating oscillating forces due to vortex shedding, for example, a sword sweeping through the air. A physically derived model was implemented enabling accurate sound synthesis results with real-time operation. Semi-empirical equations from fluid dynamics were used in [6] to calculate frequencies and other acoustic properties. The results of this paper were extended to include mechanical properties in [7]. A similar approach is undertaken in this paper.

This work is related to the fluid dynamics of flue instruments, like the pipe organ [8], where the pipe mode resonance is similar to that of a deep cavity, (see Section 4.1). Instead of being coupled to a cavity tone these instruments have an air jet striking a wedge which generates the edge tone [9].

3. PROBLEM FORMULATION

The goal is to create an accurate cavity tone sound effect that operates in real-time. The parameters that we wish a user to be able to adjust are cavity dimensions, airspeed and listener position. The important aspects of the tones produced by air flowing over a cavity are the frequency components, magnitude of propagation based on observer's distance and angle, and the bandwidth of the tones. The purpose of the research is to create a sound synthesis model of a fundamental aeroacoustic sound source which can then be used as an integral component of practical models, for example a wheel well as part of an aircraft model.

Semi-empirical equations defined or derived from fundamental fluid dynamics principles have been created and used by aeroacoustic engineers to diminish complex computations yet provide accurate acoustic results. Relevant equations from this field have been identified, based on tangible parameters, allowing us to build a physical model sound effect. Should explicit equations not exist then approximate ones based on observations from previously published results are implemented.

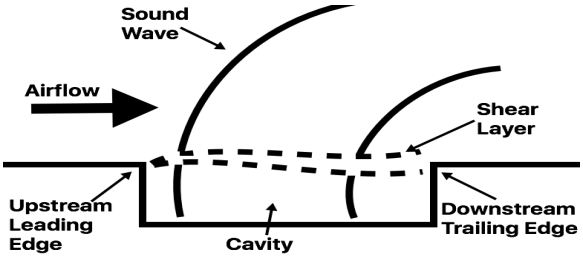

Figure 1: Basic components of cavity used in tone generation.

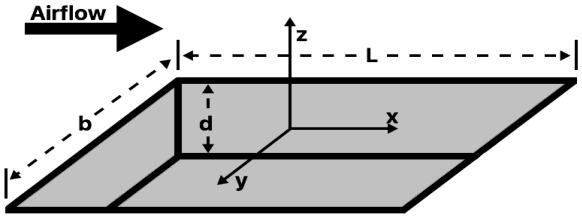

Figure 2: Diagram showing coordinates of a cavity.

4. BACKGROUND THEORY OF CAVITY TONE

4.1. Basic Principals

The generation of an acoustic tone due to air flowing over the open side of a cavity is described in [10–12]. Figure 1 illustrates air flowing over a cavity. As air passes over the leading edge vortices are generated due to the difference in airspeed between the free stream air and air in the cavity. The region of vortices is called the *shear layer*.

There are two operating modes exhibited by cavities: shear mode and wake mode. The shear mode is when the 3 dimensional shear layer collides with the trailing edge in a flapping motion. The wake mode is far less common and where a large 2 dimensional vortex is shed from the cavity itself. This report is focused on the shear mode.

As the vortices in the shear layer travel to the far side of the cavity they collide with the trailing edge generating an acoustic pressure wave. Outside the cavity the pressure wave propagates to the far field and is perceived as sound. Inside the cavity the pressure waves travel back towards the leading edge, interacting with the vortices being shed, re-enforcing the shedding process and creating a feedback system. The dimensions of the cavity used in this paper are shown in Fig. 2.

A shallow cavity is described in [13] as having the dimension ratio L/d > 1. Similariy a deep cavity has dimensions L/d <1. Shallow cavities are dominated by a dipole sound source while deep cavities are dominated by the cavity resonance tone which is monopole in nature. [14] states the contribution from cavity resonance is important for deep cavities only and when the ratio L/d > 5/2 these resonances can dominate the acoustic radiation. The width *b* of the cavity only affects the frequency of the cavity resonance and has no effect on the feedback system.

Dipoles and monopoles are compact sound sources used to represent the sounds generated when the distance between observer and source is small compared to the sound wavelength. A monopole is a pulsating sphere radiating spherical waves while a dipole is a sphere oscillating from side to side.

Shallow cavities are either open or closed. Open cavities are

when the shear layer re-attaches around the trailing edge, as shown in Fig. 1. A closed cavity is a longer shallow cavity when the shear layer attaches to the bottom of the cavity prior to the trailing edge and does not produce the same dipole output. The shear layer should always reattach to the trailing edge in a deep cavity.

A condition that can indicate whether a cavity is closed or open is the ratio between the length and depth. [15] found that cavities become closed when the ratio $L/d > 8$, whilst quoting a separate study which found $L/d > 11$.

4.2. Frequency Calculations

In 1878 the Czech physicist Vincenc Strouhal defined one of the fundamental relationships of fluid dynamics which linked a physical dimension L, airspeed u and frequency f of the tone produced to a dimensionless variable known as the Strouhal number S_t. This is given in Eqn 1:

$$f = \frac{S_t u}{L} \tag{1}$$

where for the case of the cavity tone, L represents the cavity length. The first main research that predicted the cavity tone frequencies was done by Rossiter [10] defining the following formula to determine the Strouhal number:

$$S_{t_\lambda} = \frac{\lambda - \alpha}{\frac{1}{K} + M} \tag{2}$$

where α is a constant representing the difference in phase between the acoustic wave arriving at the leading edge and the vortex being shed. It was fitted to the measured experimental data and a value of 0.25 was found. The constant K represents the ratio of convection velocity of vortices to the free stream flow speed. Rossiter gave K the value of 0.57, again to fit the observed data. λ is an integer number representing the mode.

Rossiter's equation, Eqn. 2, was extended by Heller et al. [16] to include the correction for the speed of sound within the cavity. This is shown in Eqn. 3

$$S_{t_\lambda} = \frac{\lambda - \alpha}{\frac{1}{K} + \frac{M}{[1+\frac{\gamma-1}{2}M^2]^{\frac{1}{2}}}} \tag{3}$$

where γ is the ratio of specific heats; [16] gives $\gamma = 1.4$. Rewriting Eqn. 1 to include the Strouhal number calculated by Eqn. 3 we obtain the frequency of each Rossiter mode f_λ:

$$f_\lambda = \frac{\lambda - \alpha}{\frac{1}{K} + \frac{M}{[1+\frac{\gamma-1}{2}M^2]^{\frac{1}{2}}}} \frac{u}{L} \tag{4}$$

4.3. Acoustic Intensity Calculations

Pioneering research into aeroacoustics was carried out by Lighthill [17, 18] who took the fundamental fluid dynamics equations, Navier Stokes equations, and defined them for the wave equation to predict the acoustic sound. In [14] Howe uses a Green's Function to solve Lighthill's Acoustic Analogy in relation to the acoustic intensity of cavity tones. This solution provides a relationship defining the acoustic intensity based on the tone frequency, airspeed, cavity dimensions and propagation angle. The Green's function has components relating to a dipole field generated by the feedback system G_D and a monopole field created by the cavity resonance G_M.

Using the the Green's function Howe [14] derived the non-dimensional far field acoustic pressure frequency spectrum, $\Phi(\omega, x) \approx$

$$\frac{M^2(\omega\delta^*/U)^{5/3}}{(1+M\cos\phi)^2\{(\omega\delta^*/U)^2+\tau_p^2\}^{3/2}} \left|\frac{C_2\sin(\kappa d)}{\cos\{\kappa(d+\zeta+\mathrm{i}(\kappa A/2\pi))\}} + \mathrm{i}(\cos\phi - M)\right|^2 \tag{5}$$

where x is the distance along the x axis of the cavity. The first and second terms in the magnitude brackets correspond to the monopole and dipole radiation respectively. $A = bL$ is the area of the cavity mouth, τ_p is a constant set to 0.12 and ζ is an *end correction* set to $\sqrt{\pi A/4}$. The end correction is the effective length to which the cavity must be extended to account for the inertia of fluid above the mouth of the cavity also set into reciprocal motion by the cavity resonance (see [14] for a more detailed explanation).

A fixed value for δ^* is set in [14], making the second Rossiter frequency dominant. The value of δ^* has a large influence over the dominant mode [19]. Dipole sources model Rossiter modes, with frequencies obtained from Eqn 4. The monopole source frequency, relating to the lowest order mode, is calculated when the complex frequency satisfies:

$$\kappa\left(d + \zeta + \mathrm{i}\frac{\kappa A}{2\pi}\right) = \frac{\pi}{2} \tag{6}$$

4.4. Tone Bandwidth

To date no research has been found that describes the relationship between the peak frequency and the bandwidth of the tone. The Reynolds number is a dimensionless measure of the turbulence in a flow given by:

$$R_e = \frac{\rho_{air}\, d\, u}{\mu_{air}} \tag{7}$$

It is known that the higher the Reynolds number, the smaller scale the vortices will be. This would imply that the higher the Reynolds number the wider the tone bandwidth.

5. IMPLEMENTATION

The equations in this section are discrete compared to the continuous formulas previously stated. The discrete time operator $[n]$ has been omitted until the final output (section 5.6), to reduce complexity. It should be noted that the airspeed u is sampled at 44.1KHz to give $u[n]$ and hence, $M[n], \omega[n], \kappa[n], St[n], f[n], Re[n], \Phi[n], \delta^*[n], Q[n]$ and $a[n]$.

Our synthesis model was implemented using the software Pure Data. This was chosen due to the open source nature of the code and ease of repeatability rather than high performance computations. Airspeed, cavity dimensions and observer position are adjustable in real-time. Properties like air density, speed of sound etc., are set as constants for design purposes but can be adjusted with minimal effort if a real-time evolving environment is required. All intermediate calculations are performed in real-time and no preprocessing is required.

Table 1: Values of the ratio L/θ_0 for different L/d values.

Reference	L/d	L/θ_0
[19]	2	52.8
	4	60.24
	4	86.06
	6	90.36
[20]	4	82

5.1. Conditions of Activation

The change from open to closed cavity occurs when the length to depth ratio passes a value around $L/d > 8 \rightarrow 11$ (Section 4.1). This is implemented by a sigmoid function, indicating whether the cavity is open or closed when L/d passes a value between 8 and 11. If the cavity is flagged as closed then Rossiter mode dipoles do not produce and sound.

5.2. Frequency Calculations

A discrete implementation of Eqn. 4 is used with $\lambda = [1, 4]$ to give the first 4 Rossiter frequencies $f_{D\lambda}$. These relate to the dipole sources associated with the feedback loop.

To calculate the monopole resonant mode frequency a solution to the real part of Eqn. 6 is found; shown in Eqn. 8:

$$\kappa(d + \zeta) = \frac{\pi}{2} \tag{8}$$

with $\kappa = \omega/c$ and $\omega = 2\pi f_M$. Rearranging reveals the monopole frequency, f_M as:

$$f_M = \frac{c}{4(d + \zeta)} \tag{9}$$

5.3. Shear Layer Thickness

[19] and [20] state values for the ratio of L/θ_0 and d/θ_0 for a number of different ratios of L/d. These are shown in Table 1. A linear regression line is calculated for this data giving the relationship:

$$\frac{L}{\theta_0} = 9.39\frac{L}{d} + 36.732 \tag{10}$$

Since the parameters L and d are set we can calculate a predicted value for θ_0. The shear layer effective thickness at separation, δ_0^* and θ_0 are related by Eqn. 11 [21]:

$$H = \delta_0^*/\theta_0 \tag{11}$$

where H is a *shape factor* given in [20] as 1.29 for turbulent flow and 2.69 for laminar. Using Eqn. 10 and the relationship with the shape factor we are able to calculate δ_0^*.

The shear layer thickness over the cavity δ_c is stated in [21] and given as:

$$\delta_c = \left(\frac{xL}{R_{e_L}}\right)^{\frac{1}{2}} \tag{12}$$

for a laminar flow, where R_{e_L} is the Reynolds number with respect to the cavity length. For turbulent flow,

$$\delta_c = \left(\frac{x}{\sigma\sqrt{8}}\right) \tag{13}$$

where σ is the *Gortler Parameter* calculated from [19] to lie between 5 and 7. We chose $\sigma = 6$ for this model. x is the distance along the cavity length. We need to select a value of x to obtain the shear layer thickness for the calculations. Since the dipole is positioned near the trailing edge [19], we set $x = 0.75L$.

The relationship between δ^* and δ is given in [21] as:

$$\delta^* = \frac{1}{1 + n}\delta \tag{14}$$

where $n = 7$. From Eqn. 14 we can calculate δ_c^* using δ_c as found from either Eqn. 12 or 13. The total shear layer effective thickness is obtained from Eqn. 15.

$$\delta^* = \delta_c^* + \delta_0^* \tag{15}$$

A critical value for R_{e_L} of 25000 is set [22], and implemented with a sigmoid function providing a transition from laminar to turbulent flow.

5.4. Acoustic Intensity Calculations

The acoustic intensity is calculated from a real-time discrete version of Eqn. 5 for the previously calculated monopole and dipole frequencies, Eqn. 9 and a discrete version of Eqn. 4. To achieve this the real and imaginary parts of the equation within the magnitude brackets are separated out. The denominator of the first component is:

$$\cos\left[\kappa\left(d + \zeta + \mathrm{i}\frac{\kappa A}{2\pi}\right)\right] \tag{16}$$

multiplying κ into the brackets becomes:

$$\cos\left[\kappa(d + \zeta) + \mathrm{i}\left(\frac{\kappa^2 A}{2\pi}\right)\right] \tag{17}$$

Using the identity:

$$\cos(a + \mathrm{i}b) = \cos a\frac{e^b + e^{-b}}{2} - \mathrm{i}\sin a\frac{e^b - e^{-b}}{2}$$

Let

$$X = \cos\left[\kappa(d + \zeta)\right]\left[\frac{e^{\left(\frac{\kappa^2 A}{2\pi}\right)} + e^{-\left(\frac{\kappa^2 A}{2\pi}\right)}}{2}\right]$$

$$Y = \sin\left[\kappa(d + \zeta)\right]\left[\frac{e^{\left(\frac{\kappa^2 A}{2\pi}\right)} - e^{-\left(\frac{\kappa^2 A}{2\pi}\right)}}{2}\right]$$

Expanding the magnitude brackets, the discrete implementation of Eqn. 5 becomes:

$$\Phi(\omega, x) \approx \frac{M^2(\omega\delta^*/U)^{5/3}}{(1 + M\cos\phi)^2\{(\omega\delta^*/U)^2 + \tau_p^2\}^{3/2}} \left[\left[\frac{XC_2\sin(\kappa d)}{X^2 + Y^2}\right]^2 + \left[\frac{YC_2\sin(\kappa d)}{X^2 + Y^2} + (\cos\phi - M)\right]^2\right] \tag{18}$$

Howe [14] gives a value of $C_2 = 1.02$ for a cavity with d/L ratio $= 0.5$ and τ_p is given as 0.12. To enable us to identify gains for the dipole sounds and monopole sound the second element within the large brackets is expanded giving:

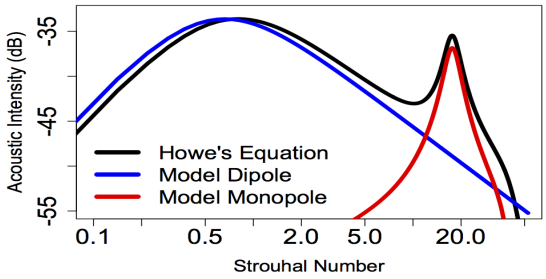

Figure 3: Far field spectrum gains calculated by Eqn. 20 & Eqn. 21 as compared to Howe's derivation from [14]. $L = b = 0.03m$, $d = 0.015m$ and $u = 3.43m/s$.

$$\left(\frac{YC_2\sin(\kappa d)}{X^2+Y^2}\right)^2 + 2\left(\frac{YC_2\sin(\kappa d)}{X^2+Y^2}(\cos\phi - M)\right) + (\cos\phi - M)^2 \tag{19}$$

It is seen that the middle term in Eqn. 19 contains elements from both monopole and dipole sources. Since the monopole is the more efficient compact source [23] this term is included in the monopole equation to minimise error. The monopole gain is shown in Eqn. 20:

$$G_M(\omega_M, r, \phi) \sim \frac{M^2(\omega_M\delta^*/U)^{5/3}}{r(1+M\cos\phi)^2\{(\omega_M\delta^*/U)^2+\tau_p^2\}^{3/2}} \left[\left[\frac{XC_2\sin(\kappa_M d)}{X^2+Y^2}\right]^2 + \left[\frac{YC_2\sin(\kappa_M d)}{X^2+Y^2}\right]^2 + 2\frac{YC_2\sin(\kappa d)}{X^2+Y^2}(\cos\phi - M)\right] \tag{20}$$

where $G_M(\omega_M, r, \phi)$ is the discrete far field spectrum gain in relation to the monopole. For the dipole:

$$G_D(\omega_{D\lambda}, r, \phi) \sim \frac{M^2(\omega_{D\lambda}\delta^*/U)^{5/3}}{r(1+M\cos\phi)^2\{(\omega_{D\lambda}\delta^*/U)^2+\alpha_p^2\}^{3/2}} \left[\left[\cos\phi - M\right]^2\right] \tag{21}$$

where $G_D(\omega_{D\lambda}, r, \phi)$ is the discrete far field spectrum gain in relation to the dipole representing one of the Rossiter modes (λ). In Eqns. 20 and Eqn. 21, the distance between the source and listener, r, represents how the sound amplitude diminishes with respect to distance in the far field. Figure 3 shows the output from Eqns. 5, 20 and 21, with $r = 1$.

5.5. Tone Bandwidth

As stated in Section 4.4, no exact relationship for the tone bandwidth has been found. It is known that the higher the Reynolds number the more the vortices reduce in size with increased complex interactions leading to a broader width around the peak frequency; laminar flow will have larger, simpler interactions and be closer to a pure tone.

Table 2: Q values with corresponding Reynolds numbers measured from plots given in publications.

Reference	Q	R_{e_L}
[13]	5	5.64 x 10^5
	4.5	4.52 x 10^5
	4.5	3.45 x 10^5
[24]	25	3.10 x 10^5
[25]	11.875	1.27 x 10^5
[26]	6	1.47 x 10^5
	14	3.54 x 10^6
	14	7.08 x 10^6
[27]	6.875	2.48 x 10^6
	7.875	2.95 x 10^6
[28]	22.5	4.01 x 10^6
[29]	76	4.51x 10^4
[30]	15	6.46 x 10^5

In signal processing the relationship between the peak frequency and bandwidth is called the Q value, ($Q = f_{D\lambda}/\Delta f$, where Δf is the tone bandwidth at -3dB of the peak). To approximate the relationship between Q and R_{e_L}, the peak frequencies and bandwidths from previously published plots are measured [13, 24–30]. Results are shown in Table 2.

A linear regression line, fitted to the natural logarithm of the Reynolds number, was obtained from the data in Table 2. The equation is given in Eqn. 22:

$$Q = 87.715 - 5.296\log(R_{e_L}) \tag{22}$$

To prevent Q reaching unrealistic values a limit has been set so that $2 \leq Q \leq 90$.

5.6. Total Output

The implementation described above determines the values used in the final output. The sound is generated from a noise source shaped by a number of bandpass filters. A flow diagram of the synthesis process for a dipole source is shown in figure 4. It can be seen from Fig. 4 how the parameters are interrelated through the different semi-empirical equations ensuring accuracy throughout the sound effect characteristics.

The monopole source frequency due to the depth resonant mode $f_M[n]$ is calculated from Eqn. 9. The noise source is filtered through a bandpass filter with the centre frequency set at $f_M[n]$, Q value set by Eqn. 22, giving the output from the filter, $B_M[n]$. The intensity is calculated from Eqn. 20 as $G_M(\omega_m[n], r, \theta)$, where $\omega_m[n] = 2\pi f_M[n]$, giving total monopole output, $M[n]$:

$$M[n] = G_M(\omega_m[n], r, \theta)B_M[n] \tag{23}$$

The dipole frequencies due to the Rossiter modes are set from a discrete implementation of Eqn. 3 with $\lambda = [1, 4]$; the corresponding frequency values, $f_{D\lambda}[n]$ are calculated from Eqn. 4. The noise source is filtered through a bandpass filter with the centre frequency set at $f_{D\lambda}[n]$, Q value set by Eqn. 22, giving the output from the filter, $B_{D\lambda}[n]$. The intensity is calculated from Eqn. 21 giving a single dipole output, $D_\lambda[n]$:

$$D_\lambda[n] = G_D(\omega_{D\lambda}[n], r, \theta)B_{D\lambda}[n] \tag{24}$$

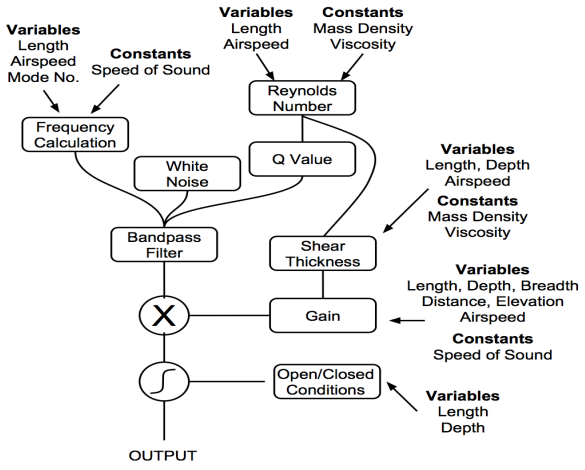

Figure 4: Flow diagram showing typical dipole synthesis process

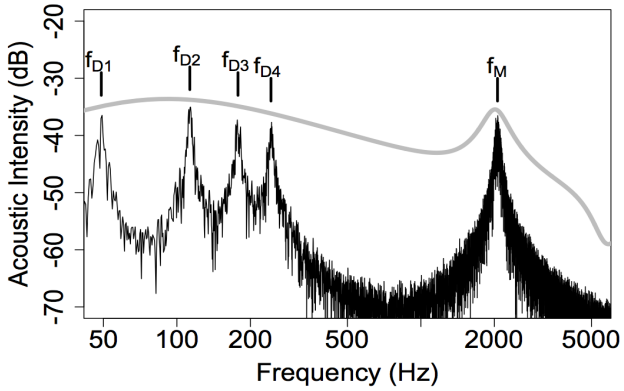

Figure 5: Output from the cavity synthesis model. The grey line indicates the value from Eqn. 5 for comparison. L and b = 0.03m, d = 0.015m, u = 3.43m/s, $\theta = 30^\circ$.

where $\omega_m[n] = 2\pi f_D[n]$. The total output for the cavity tone $y[n]$ is given as the summation of the output of the resonant monopole and dipoles representing the first 4 Rossiter modes, shown in Eqn. 25;

$$y[n] = M[n] + D_1[n] + D_2[n] + D_3[n] + D_4[n] \qquad (25)$$

6. RESULTS

Figure 3 illustrates the outputs from Eqns. 20 and 21 as compared to that given by [14]. The peak gain value occurs at a slightly lower Strouhal number in our model than in Howe's equation 5. The difference is most likely due to the way the boundary layer thickness is calculated, which is fixed in [14] but varies due to changing conditions in our model.

The plot of the monopole output from our model matches well with that given in [14]. This indicates, for this airspeed, the additional component added in to Eqn 20 containing a dipole term does not diminish accuracy.

Comparison of the model's frequency calculations to previously published results is shown in Table 3. No specific frequencies are published in [14] but our model shows good agreement with the dominant peak indicated in [14] and the second dominant mode from the model. Our model is designed around the theory presented in [14] and hence a close result was expected.

There are several results presented in [13]; the emphasis of that publication is to provide benchmark data to validate computational aeroacoustic codes. Our physical synthesis model obtains excellent results compared to [13]. The results from our model for the lowest airspeeds (89.2 m/s and 137.2 m/s) are closer to the theoretical predictions while the higher airspeeds are all closer to the published wind tunnel results. The difference between results pertaining to the lower speeds and the higher speed is most likely due to the use of Rossiter's formula in [13]; our model uses Eqn. 3 while [13] uses Eqn. 2.

Results presented in [31] are in relation to a larger sized cavity. Although the published measured, computational and theoretical results are all close, they do highlight the difference in all three methods. It can be seen that results from our model lie within the range of all the published results. The monopole due to cavity resonance is found to be dominant under these conditions in our model.

The difference between the three results; measured, theoretical and computational, is again highlighted in [32]. The frequencies presented here are higher than perceptible by the human ear but are useful to see how our model performs under these conditions. Again it can be seen that the published theoretical results and our model results are similar but the measured / computational results are slightly higher.

A deep cavity is tested in [24] at a subsonic airspeed; the Rossiter frequencies are not published. The cavity resonance is dominant in our physical model at a frequency of 213Hz, close to the published result of 225Hz. This indicates that our model is accurate when calculating the monopole frequency as well as the Rossiter frequencies, with similar discrepancies previously between measured and theoretical results.

Examination of low airspeed over a wide cavity is examined in [33] as a comparison to a measurement technique called Particle Image Velocimetry, (beyond the scope of this paper). Results indicate a more pronounced difference between the frequencies from this publication to those from our model. Our model correctly predicts the dominant modes but gives noticeably lower frequencies, especially for the 12 m/s case. It is known that theoretical models are less accurate at very low air speeds and at the same time the variation in measured frequencies is much wider [20].

The last example is from [34] when a cube shaped cavity is tested. The results are read from a graph but it can be seen that the values from our model are lower than the published values. For these dimensions the monopole due to cavity resonance is dominant, not the Rossiter frequencies. This is not altogether unexpected since it was stated that if $L/d > 5/2$ resonances can dominate [14], (section 4.1).

Comparing our model's average frequency prediction to published results we found it was 0.3% lower than theoretical frequencies, 2.0% lower than computed frequencies and 6.4% lower than measured frequencies.

An example output of the cavity tone synthesis model is shown in Fig. 5 indicating f_{D1}, f_{D2}, f_{D3} and f_{D4} where f_{D2} is the dominant mode. The conditions are set to match the example given by Howe [14]. The monopole output is clearly visible at the same frequency as calculated by Howe's equation.

Table 3: Comparison of published measured, computed and theoretical results and our synthesis model. ***Bold*** indicates dominant frequency. Ref. = Reference. (* - read from a graph, † - theoretical answer, ‡ - computational answer, ? - Unknown)

Ref.	**Airspeed (m/s)**	**Dimensions (m)**			**Published Results (Hz)**					**Physical Model Results (Hz)**				
	u	l	w	d	f_{D1}	f_{D2}	f_{D3}	f_{D4}	f_M	f_{D1}	f_{D2}	f_{D3}	f_{D4}	f_M
[14]	3.43	0.03	0.03	0.015		114*†				49	**113**	178	243	2061
[13]	89.2	0.0191	0.1016	0.0127		4530 4063†				1739	**4057**	6376	8695	1656
	137.2					5854†				2506	**5848**	9190	12532	
	181.8					7339 8062†				3141	**7330**	11519	15707	
	230.5					8809 9401†				3773	**8804**	13835	18865	
	274.4					10027 10372†				4294	**10019**	15745	21470	
	308.7					10925 10941†				4680	**10919**	17159	23398	
[31]	291.6	0.4572	0.1016	0.1016	195 181† 193‡	419 422† 460‡	693 663† 667‡	947 904† 940‡		188	438	689	938	**293**
[32]	514.5	0.0045	?	0.0015	31899 28469† 32242‡	71344 66542† 66542‡	110789 104615† 126567‡			28567	66657	**104707**	142837	
[24]	40	0.06	0.06	0.35					225	267	623	980	1336	**213**
[33]	12	0.03	0.6	0.015		**454** **454**‡		908 908‡		168	**391**	615	838	640
	15					**496** **496**‡		992 992‡		209	**487**	766	1043	
[34]	31	0.15	0.15	0.15	125*	245*	**375***			84	196	308	420	**303**

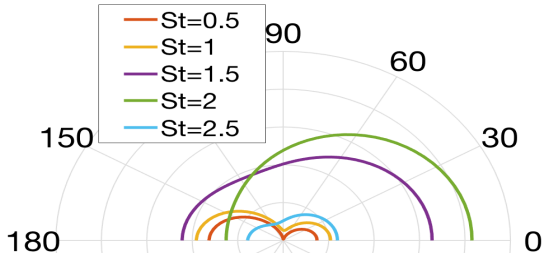

Figure 6: Directional output from synthesis model. L and b = 0.03m, d = 0.015m, airspeed = 34.3m/s. St = Strouhal number.

The directional output is shown in Fig. 6. For different Strouhal numbers there are different propagation angles. The propagation becomes more circular as the frequency increases, indicating the influence of the monopole. Comparing Fig. 6 with published results by Howe [14] indicates that for our model the circular monopole occurs at $St \approx 2$ whereas it occurs at $St \approx 2.5$ in [14].

7. DISCUSSION

The formula given in [16], implemented by our model, performs well for frequency prediction compared to the previously published results in Table 3 obtained through wind tunnel measurements, theoretical predictions and computational fluid dynamics. The papers with more than one result for the same conditions highlight that it is difficult to predict an exact frequency value from theory, indicating that the theoretical and computational models may not capture all the underlying fluid dynamic processes ongoing when a cavity tone is produced. The wind tunnel recordings may also have been affected by noise and interference from equipment and the tunnel itself.

The values of C_2 and τ_p introduced by Howe [14] in Eqn. 5 may change depending on the cavity dimensions. If so, this would introduce discrepancies between our model and measured outputs.

The acoustic intensity calculated by the model matches well with the theory introduced by Howe [14]. The sound effect is given an independent gain to allow sound designers to achieve the loudness they desire while maintaining the relationships over the frequency range and if combining multiple compact sources.

The directional output from our model is like that produced by Howe [14] but is found to differ at higher strouhal numbers. The cause of this is unknown as there is no difference between the theoretical equation identified by Howe for directional propagation and the equation implemented in the physical model.

The equation from Howe [14], Eqn. 5, takes into account the elevation of the observer to the tone. It does not take into consideration the azimuth angle making the radiated output inherently 2 dimensional rather than 3D. The calculation of the acoustic resonance frequency of the cavity is still based on three dimensions.

This research focused on the sound generated from a cavity as the air passes over it parallel to the length dimension, (Fig. 2). The vast majority of research by the fluid dynamics community

has this condition due to the need to minimise noise generated by wheel wells or bomb bay doors in aircraft. This physical model can be used to calculate the sound produced by cavities under such circumstances. The physics change when there is an angle of attack on the incoming air which is beyond the scope of this paper.

Other sound effects that can be developed in the future using our model as a component part could range from a pipe organ to grooves in the cross section of a sword. The model may also be used to calculate the sound generated by a car travelling with a sunroof or window open or wind passing doorways and other exposed cavities.

A demo of our cavity tone synthesis model is available at https://code.soundsoftware.ac.uk/hg/cavity-tone.

8. CONCLUSIONS

We have developed a compact sound source representing the cavity tone based on empirical formulas from fundamental fluid dynamics equations. This has produced a sound synthesis model which closely represents what would be generated in nature. The model operates in real-time and unlike other models, our approach accounts for the angle and distance between source and receiver. Although the solution presented is less detailed than solutions obtained from CFD techniques, results show that the model predicts frequencies close to measured and computational results however unlike other methods our model operates in real-time.

Acoustic intensity and propagation angles derived from fundamental fluid dynamics principles are implemented which overall have good agreement with published results.

9. ACKNOWLEDGMENTS

Supported by EPSRC, grant EP/G03723X/1. Thanks to Will Wilkinson, Brecht De Man, Stewart Black and Dave Moffat for their comments.

10. REFERENCES

[1] Y Dobashi, T Yamamoto, and T Nishita. Real-time rendering of aerodynamic sound using sound textures based on computational fluid dynamics. In *ACM Transactions on Graphics*, California, USA, 2003.

[2] D Berckmans et al. Model-based synthesis of aircraft noise to quantify human perception of sound quality and annoyance. *Journal of Sound and Vibration*, Vol. 331, 2008.

[3] A Farnell. *Designing sound*. MIT Press Cambridge, 2010.

[4] S Bilbao and CJ Webb. Physical modeling of timpani drums in 3d on gpgpus. *Journal of the Audio Engineering Society*, Vol. 61, 2013.

[5] F Pfeifle and R Bader. Real-time finite difference physical models of musical instruments on a field programmable gate array. In *Proc. of the 15th Int. Conference on Digital Audio Effects*, York, UK, 2012.

[6] R Selfridge et al. Physically derived synthesis model of an Aeolian tone. In *Audio Engineering Society Convention 141*, Los Angeles, USA, Best Student Paper Award. 2016.

[7] R Selfridge, DJ Moffat, and JD Reiss. Real-time physical model of an Aeolian harp. In *24th International Congress on Sound and Vision (accepted)*, London, UK, 2017.

[8] JW Coltman. Jet drive mechanisms in edge tones and organ pipes. *The Journal of the Acoustical Society of America*, Vol. 60, 1976.

[9] MS Howe. Edge, cavity and aperture tones at very low mach numbers. *Journal of Fluid Mechanics*, Vol. 330, 1997.

[10] JE Rossiter. Wind tunnel experiments on the flow over rectangular cavities at subsonic and transonic speeds. Technical report, Ministry of Aviation; Royal Aircraft Establishment; RAE Farnborough, 1964.

[11] CKW Tam and PJW Block. On the tones and pressure oscillations induced by flow over rectangular cavities. *Journal of Fluid Mechanics*, Vol. 89, 1978.

[12] T Colonius, AJ Basu, and CW Rowley. Numerical investigation of flow past a cavity. In *AIAA/CEAS Aeroacoustics Conference*, Seattle, USA, 1999.

[13] KK Ahuja and J Mendoza. Effects of cavity dimensions, boundary layer, and temperature on cavity noise with emphasis on benchmark data to validate computational aeroacoustic codes. Technical report, NASA 4653, 1995.

[14] MS Howe. Mechanism of sound generation by low mach number flow over a wall cavity. *Journal of sound and vibration*, Vol. 273, 2004.

[15] V Sarohia. Experimental investigation of oscillations in flows over shallow cavities. *AIAA Journal*, Vol. 15, 1977.

[16] HH Heller, DG Holmes, and EEE Covert. Flow-induced pressure oscillations in shallow cavities. *Journal of sound and Vibration*, Vol. 18, 1971.

[17] MJ Lighthill. On sound generated aerodynamically. i. general theory. *Proc. of the Royal Society of London. Series A. Mathematical and Physical Sciences*, 1952.

[18] MJ Lighthill. On sound generated aerodynamically. ii. turbulence as a source of sound. In *Proc. of the Royal Society of London A: Mathematical, Physical and Engineering Sciences*, 1954.

[19] CW Rowley, T Colonius, and AJ Basu. On self-sustained oscillations in two-dimensional compressible flow over rectangular cavities. *Journal of Fluid Mechanics*, Vol. 455, 2002.

[20] V Suponitsky, E Avital, and M Gaster. On three-dimensionality and control of incompressible cavity flow. *Physics of Fluids*, Vol. 17, 2005.

[21] T Cebeci and P Bradshaw. *Physical and computational aspects of convective heat transfer*. Springer Science & Business Media, 2012.

[22] H Schlichting et al. *Boundary-layer theory*. Springer, 1960.

[23] D G Crighton et al. *Modern methods in analytical acoustics: lecture notes*. Springer Science & Business Media, 2012.

[24] DD Erickson and WW Durgin. Tone generation by flow past deep wall cavities. In *25th AIAA Aerospace Sciences Meeting*, Reno, USA, 1987.

[25] YH Yu. Measurements of sound radiation from cavities at subsonic speeds. *Journal of Aircraft*, Vol. 14, 1977.

[26] HE Plumblee, JS Gibson, and LW Lassiter. A theoretical and experimental investigation of the acoustic response of cavities in an aerodynamic flow. Technical report, DTIC Document, 1962.

[27] J Malone et al. Analysis of the spectral relationships of cavity tones in subsonic resonant cavity flows. *Physics of Fluids*, Vol. 21, 2009.

[28] CW Rowley et al. Model-based control of cavity oscillations part ii: system identification and analysis. In *40th AIAA Aerospace Sciences Meeting & Exhibit*, Reno, USA, 2002.

[29] K Krishnamurty. Acoustic radiation from two-dimensional rectangular cutouts in aerodynamic surfaces. *NACA Technical Note 3487*, 1955.

[30] N Murray, E Sällström, and L Ukeiley. Properties of subsonic open cavity flow fields. *Physics of Fluids*, Vol. 21, 2009.

[31] D Fuglsang and A Cain. Evaluation of shear layer cavity resonance mechanisms by numerical simulation. In *30th Aerospace Sciences Meeting and Exhibit*, Reno, USA, 1992.

[32] X Zhang, A Rona, and JA Edwards. An observation of pressure waves around a shallow cavity. *Journal of sound and vibration*, Vol. 214, 1998.

[33] V Koschatzky et al. High speed PIV applied to aerodynamic noise investigation. *Experiments in fluids*, Vol. 50, 2011.

[34] L Chatellier, J Laumonier, and Y Gervais. Theoretical and experimental investigations of low mach number turbulent cavity flows. *Experiments in fluids*, Vol. 36, 2004.